Can we resolve the basin-scale sea-level budget from GRACE ocean mass?

Sam Royston[1], Bramha Dutt Vishwakarma[1], Richard Westaway[1], Jonty Rougier[2], Zhe Sha[1,2], Jonathan Bamber[1]

[1]School of Geographical Sciences, University of Bristol, UK
[2]School of Mathematical Sciences, University of Bristol, UK

Key Points:

- Spatial patterns of the sum of steric and ocean mass sea-level trends do not fully match those from satellite altimetry
- Misclosure due to steric data lacking short-wavelength information and hemisphere-scale differences in observation processing
- The sea-level budget closure on the global scale to some extent represents a cancellation of errors

Corresponding author: Sam Royston, `s.royston@bristol.ac.uk`

Abstract

Understanding sea-level changes at a regional scale is important for improving local sea-level projections and coastal management planning. Sea-level budget (SLB) estimates derived from the sum of observation of each component close for the global mean but at the local to ocean basin scale this is not the case. The sum of steric and mass contributions to sea level calculated from measurements of these components does not match the spatial patterns of sea surface height trends from satellite altimetry over the period 2005–2015. We investigate potential drivers of this mis-match and find that the steric and mass observation systems do not represent the small-scale features seen in the satellite altimetry. In addition there are discrepancies apparent at the global and hemispheric scale, which are most likely due to orbit and geocenter motion errors. While it is expected that the small-scale discrepancies should cancel out when averaging over an ocean basin or globally, we find that spatially-averaging the (area-weighted) trends gives poorer agreement than averaging the sea-level anomaly (SLA) time series into a basin mean to then calculate an aggregated trend. Therefore, caution should be taken when analysing contributions to sea-level variations from spatially-distributed observations rather than aggregating time series first. Discrepancies in the SLB are worst for the Indian-South Pacific Oceans. We conclude that the SLB closure on the global scale to some extent represents a cancellation of errors.

Plain Language Summary

An important check on the accuracy of our global measurement systems and understanding of the processes driving sea-level rise is the sea-level budget. This describes the comparison of measured sea surface height change from satellite radar altimetry with the sum of its component parts, due to density and mass changes. With over 11 years of very high quality density and mass observations at good spatial scale, the sum of the parts matches the total within some uncertainty at a global scale. If, however, we examine the sea-level budget at the ocean basin scale, we find significant discrepancies that are difficult to explain. We investigate different processing and averaging methods. We find the density measurements do not include small spatial scales that sea surface height measurements do record. Rather than this mis-match averaging out over basin scales, which we expect if the errors are random, it leads to differences in the ocean basin average. Also there is a mis-match at the hemispheric and global scale which we believe comes from the way the satellite measurements are processed.

1 Introduction

Closure of a regional to local-scale sea-level budget (SLB; e.g. Church et al. (2011)) is important to understand the accuracy of observational systems at their operational resolution, and to improve understanding and projections of sea-level change and its impacts at the coast, which is the most critical location in terms of human impacts.

At the global-scale, the SLB closes to within the uncertainty of the observations during the satellite era (WCRP, 2018). It should also be possible to reconstruct sea surface height anomalies (SSHA), derived from satellite altimetry, from the sum of steric and mass observations over a specified area. Steric data are provided by the ARGO float array but there are large uncertainties outside of their coverage in time (pre-2005) and space (deeper than 2,000 m and in sparsely monitored regions such as the polar oceans). Different processing choices in standard gridded products also have an impact at the regional scale (Storto et al., 2017). Sea-level changes due to ocean mass changes can be determined from the land mass exchange (from land ice and hydrology) applied to the sea level equation (Farrell & Clark, 1976) or they can be directly determined from gravimetry data such as from the Gravity Recovery and Climate Experiment (GRACE) mission.

Hereafter we refer to the former method as mass changes via the sea level equation and the latter as ocean-mass changes observed by GRACE. Note that these two methods should give the same global mean mass change (because of global conservation of mass) but there are large spatial variations between the different GRACE products (e.g. Dieng et al. (2015); Blazquez et al. (2018); Chen et al. (2018); WCRP (2018)). There are additionally systematic biases and hence uncertainties not accounted for in each of the observational products formal error estimates.

At the basin-scale, Frederikse et al. (2017) were able to close the SLB in most but not all basins. Their sea-level anomalies (SLAs) were defined using tide gauge data, corrected for vertical land movement by GNSS or altimetry (Wöppelmann & Marcos, 2016), and their ocean mass contribution was determined from the observed land mass change via the sea level equation. Similarly, a regional study looking specifically at the North-East Atlantic and North Sea coastlines (Frederikse et al., 2016) was able to determine a statistical relationship between tide-gauge-observed SLAs and steric SLAs in the open ocean, by removing the component due to mass. Because these studies determine ocean mass sea-level change from the sea level equation, this term represents gravitational and rotational changes but does not include changes due to ocean circulation. Yet sea level as observed by tide gauges does include ocean circulation impacts, so there is a mis-match in the contributors to the SLB that may be averaging out over the regions chosen.

A number of studies have investigated the variability of the steric and mass terms in the SLB at the basin scale, finding inter-annual variability in the seasonal signal (although the studies use short periods of data; see for example Llovel et al. (2010, 2011); Marcos et al. (2011)). Attempts to use ocean mass changes observed by GRACE in the SLB to understand basin-scale ocean circulation have also been made using short periods of data (e.g. Chambers & Willis, 2009, 2010). There have been a small number of regional studies successfully comparing changes in ocean mass, steric SLAs and SSHAs from satellite altimetry (Kleinherenbrink et al., 2016, 2017). These studies use GRACE gravimetry change to determine the mass SLA and match sub-basin-scale sea-level variability through the authors choice of products and a statistical optimisation. Purkey et al. (2014) demonstrated that basin-scale observed ocean-mass trends mostly match steric-corrected sea-level changes calculated from repeat hydrographic sections supplemented by observed SSHAs from satellite altimetry. Due to the limited spatial and temporal coverage of the hydrographic sections, the method matches the broad scale (long wavelength and longer period) trends.

To date, we are unaware of work that has successfully resolved the SLB at the regional scale using ocean-mass changes observed from GRACE.

Subjective choices regarding, for example, the data processing methodology, glacial isostatic adjustment (GIA) correction, geocentre motion correction, Earth oblateness correction and pole tide correction all have a substantial impact on ocean-mass estimates(e.g. Blazquez et al., 2018; Chen et al., 2018; Dieng et al., 2015; Jeon et al., 2018; Wahr et al., 2015). Many of these corrections affect the spatial patterns in the estimated ocean-mass trends. Of course, these systematic uncertainties in the data processing are expected to have a larger impact, proportionally, on local to regional scale observations than on the global mean. Here, we investigate the SLB at the resolution of the observational systems, using SSHA from satellite altimetry, ocean-mass changes observed by GRACE, and observational products of in-situ steric changes. With full spatial coverage and formal errors provided by satellite altimetry and gravimetry and the ARGO float program, it should in theory be possible to close the SLB at each point on the Earths surface.

2 Data and Methods

Here, we focus on the comparison of the sum of ocean-mass changes observed by GRACE and steric SLAs with SSHA from satellite altimetry. In developing the regional SLB at the ocean basin scale, we investigate the effect of different methods of calculating average and trend and the influence of different processing methods and corrections on the observations. We make comparisons of the trend spatially (i.e. on a latitude-longitude grid) and for basin-averages. Comparing the observed SSHA with mass and steric components, we decompose the residual spatially and discuss the impact of the trend calculation method versus systematic spatial uncertainties.

2.1 Data sets

The observed SSHA is determined from satellite altimetry, using the ESA SLCCI v2.0 product (Ablain et al., 2015; Legeais et al., 2018). This is a multi-mission gridded product, with high-latitude coverage and the most up-to-date instrumental and geophysical corrections applied. The SSHA is corrected for instrument and atmospheric corrections, ocean tides including long-period, solid Earth and pole tides (including the linear pole tide correction of Desai et al. (2015)) and is provided as an anomaly from the DTU15 mean sea surface. In the ESA SLCCI product, a correction of -0.3 mm y^{-1} is applied to account for the effect of GIA (Argus et al., 2014; Peltier et al., 2015) on the global scale. Because we are interested in the local spatial scale, we add the GIA correction from the ICE-6G_D VM5a model back to each ocean grid point and re-apply it at each latitude-longitude grid location from the Stokes coefficients provided by Peltier (2018) (this approach is discussed by Tamisiea (2011)). Additionally, Frederikse et al. (2017) have identified and quantified the difference between SSHA measured by altimetry and mass-driven equivalent water height changes measured by GRACE due to ocean bottom deformation (OBD). As a result of present-day land-ocean mass exchanges, the redistribution of mass leads to an elastic component of OBD on the annual to decadal scale. This deformation leads to a volume change in the ocean that is not measured by altimetry. We add a 'correction' to the altimetry data to account for the spatial distribution of this effect, using the change in the solid Easrth (crust) deformation for the same 2005–2015 period. The GIA and OBD correction rates of change are added cumulatively and linearly and then the residual bias is removed from each time series to give SSHA from a zero-mean. For completeness, in the Supplementary Information, we include comparisons with three alternative gridded satellite altimetry SSHA products, from AVISO (AVISO, 2018), MeASUREs (Zlotnicki et al., 2019) and CSIRO (CSIRO, 2019).

The steric SLA is determined as the ensemble average of four gridded, sub-surface, temperature and salinity data sets: Scripps Institution of Oceanography (hereafter SIO, updated from Roemmich & Gilson (2009)); JAMSTEC (Hosoda et al., 2008); UK Met Offices EN4.2.1 model (Good et al., 2013) with the Gouretski & Reseghetti (2010) corrections; and ISAS13 from IFREMER (Gaillard et al., 2016). These data sets use ARGO profile measurements supplemented with other sub-surface measurements from casts and profiles and are all optimal-interpolation products. The steric SLA is calculated using the Thermodynamic Equation of Sea Water (TEOS-10; Millero et al. (2008); TEOS-10 (2008)) as the equation of state. We have removed a monthly climatology defined as the time-mean for each calendar month. The uncertainty of each measurement in temperature and salinity is propagated through the TEOS-10 calculation of steric SLA to give an uncertainty for each measurement of steric SLA in each grid point time series. The ensemble mean time series of the 4 products is calculated as the weighted mean, with weights proportional to the inverse of the steric SLA error variance.

For mass SLAs we use ocean-mass observed by GRACE. The choice of data center processing and corrections applied leads to quite different global-mean trends. In this study we compare the ocean-mass equivalent water height changes from GRACE pro-

cessed by two different data centers, which cover the range of global-mean sea-level trends for the 2005-2016 period inclusive (between 2.0 and 2.6 mm y^{-1} global-mean mass sea-level equivalent; WCRP (2018), Table 11). We compare JPL mass concentration (mascon) release (RL) 05 and RL06 (Watkins et al., 2015; Weise et al., 2016; JPL, 2018; Wiese et al., 2018) and GSFC mascon RL05 (Luthke et al., 2013; Goddard Space Flight Center, 2017) products. The mascon products aim to better refine the mass changes in predefined equal-area regions of the Earth's surface and therefore due to their processing, mascon products benefit from 'cleaner data at the ocean-land boundary but have additional processing compared with spherical harmonic solutions. The JPL mascon product is defined on an equal-area grid that is 3° by 3° longitude-latitude at the equator, whereas the GSFC mascon product is defined on an equal-area grid that is 1° by 1° longitude-latitude at the equator. The native resolution of GRACE is around 300 km half-width at the equator at monthly resolution (Tapley et al., 2004; Vishwakarma et al., 2018). Therefore the JPL mascon product should have uncorrelated errors at the given mascon centers, whereas the GSFC product is provided at a smaller resolution but we expect the data to contain spatially-correlated errors. Since we are interested in the ocean-mass sea-level signal, we use the GRACE products with the AOD1B atmosphere-ocean de-aliasing model restored, but with the spatial-mean atmospheric signal at each time step removed. For the RL05 products, the Geruo A GIA model (A et al., 2013) is removed as standard whereas for the RL06 product, the ICE-6G_D VM5a GIA model (Argus et al., 2014; Peltier et al., 2015) is removed as standard. We test the sensitivity of basin-mean sea-level trends to the GIA solution chosen by adding the GIA correction back to each grid-point and subtracting different GIA forward-model corrections. We note that this approach ignores the processing steps that the data centers would make in changing GIA product and is a much simplified approach. For all basin-scale calculations, we mask and ignore spatial regions where seismic deformation after the 2004 Sumatra and 2011 Tokohu earthquakes clearly affect the ocean-mass equivalent water height observation. We omit the same mask from all observations when calculating basin-scale averages.

2.2 Method

The SSHA trend from satellite altimetry is compared to the sum of steric and mass equivalent sea-level trends. The steric sea-level trend presented hereafter is an ensemble mean of optimal-interpolation products using ARGO and other in-situ data. Ocean-mass trends are calculated from GRACE observations. To capture the longest duration of good quality data, we use monthly data from January 2005 to December 2015 inclusive. The spread in plausible values is demonstrated by varying the products used, the calculation methods and the spatial criteria for retaining data in the calculation. We compare the sea-level trend budget spatially and then aggregate by region, as defined by coherency in SSHAs observed by satellite altimetry (following Thompson & Merrifield (2014)).

The time series of each of the observed SSHA, steric SLA and GRACE observed mass SLA in each basin is determined by the area-weighted mean of latitude-longitude grid point time series. The uncertainties in each of these time series are propagated as area-weighted variance. The basin-scale linear trend in time is calculated by generalised least squares regression applied to each basin-mean time series and its uncertainty including an annual and semi-annual periodic (hereafter referred to as the time series trend). The regression includes an auto-regressive error term to account for coloured noise in each time series. We assume an auto-regressive model of order 1 (AR1) is sufficient to describe the noise in this short time series of 132 months (Bos et al., 2014; Royston et al., 2018). The data are deseasoned as part of the trend analysis except for the steric SLA where the calculation from temperature and salinity measurements to SLA accounts for the climatological monthly mean.

We additionally determine a "spatial-mean trend" where the linear trend plus annual and semi-annual periodic signals are determined by weighted least squares for each

grid point time series, with weights proportional to the inverse variance (measurement uncertainty) at each grid point. The basin-scale mean is then determined by the area-weighted average of the trends. The median value of the formal trend error estimates is taken to be representative of the trend error over the basin.

It is noted that for Figures showing spatial patterns, the data are interpolated onto the same 1° x 1° latitude-longitude grid and smoothed by a 500 km Gaussian filter for visualisation. The basin-mean trends are calculated from the latitude-longitude grid.

We investigate the power spectral density by wavelength of the contributors to, and discrepancy in, the SLB using a 2D Fourier transform applied to each data set interpolated onto the same 1° x 1° latitude-longitude grid to make a fair comparison, using Generic Mapping Tools (Wessel et al., 2013) gridfft function by spherical distance. Additionally, in the Supplementary Information, we apply spherical harmonic decomposition to the latitude-longitude gridded data.

3 Results and Discussion

The spatial variability in the sea-level trend is dominated by the steric rather than the mass signal as expected and previously reported (Leuliette & Willis (2011); Figure 1). For the study period, 2005–2015 inclusive, the steric sea-level trend is dominated by a large La Niña event in 2011 and the beginning of a large El Niño event towards the end of 2015, which give rise to the 'see-saw of trends across the Pacific (Zhang & Church, 2012). There is also a broad rise in steric sea-level trends across the Indian Ocean and South Pacific, driven by changes in wind circulation and strength over the Pacific (see for example Roemmich et al. (2016); Thompson et al. (2016a).

Visually the sum of the steric and mass sea-level trend shows largely similar patterns to the observed SSH trend (Figure 1b compared with Figure 1d,f,h), but there are clear areas of discrepancy (Figure 2a). There is an apparent basin-scale component to the discrepancy with the observed SSH trend change being larger than the sum of components in the North Indian and South Pacific Oceans and smaller than the sum in the South Indian and North Atlantic Oceans. There are large differences at a small scale that mostly cancel out with smoothing (the unsmoothed discrepancy is presented in Supplementary Figure S1), as well as specific areas of large difference such as the Agulhas Current and Gulf Stream. The smoothed spatial pattern of the discrepancy (Figure 2a) has a similar magnitude to the uncertainty introduced by processing choices, for example the difference between different GIA forward-model corrections for GRACE (Figure 2b).

It is well understood that the choice of processing and GIA forward-model can significantly affect the basin-scale SSH trend, particularly in those areas where the GIA signal has a large amplitude (e.g. Marcos et al. (2011)). It is also clear that the choice of GRACE processing produces significant variations in the trend, which corresponds with long-wavelength or low-degree spherical harmonic coefficient differences (similarly shown by Blazquez et al. (2018); Uebbing et al. (2019) and others). In our analysis, the sub-polar and sub-tropical North Atlantic basin means are most affected by the choice of GRACE product and GIA correction, with the best match given by the JPL RL06 product and ICE-6G_D VM5 GIA forward-model (Supplementary Figure S2). The difference between these models have a clear hemispheric degree-2, order-1 spherical harmonic pattern. Jeon et al. (2018) discuss the impact of different GRACE processing methods on the consistency of ocean mass estimates when compared to mass changes from the sea level equation. They suggest that improvements can be made to the RL05 standard GRACE corrections for geocenter motion, oblateness and pole tide corrections, but that there remains an inconsistency in the trend when looking at the basin scale. Our analysis, which includes the atmosphere-ocean mass variability, suggests that the changes made in RL06 of the JPL GRACE product have improved the SLB on the basin scale, particularly from

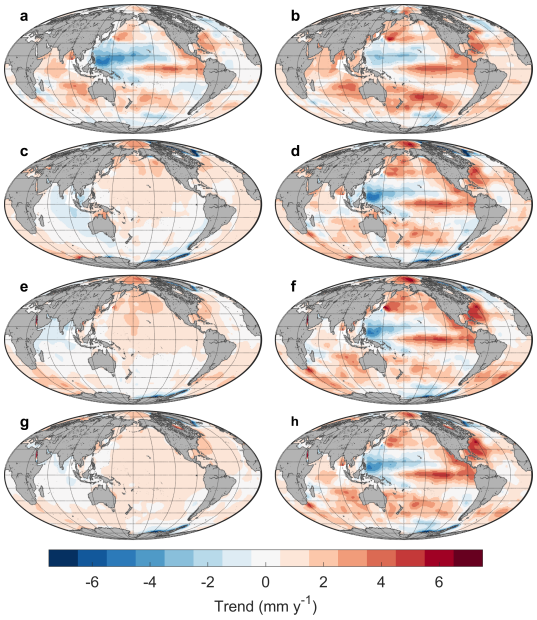

Figure 1. Trend in observed SSH (mm y^{-1}; 2005-2015 inclusive): (a) steric SSH from an ensemble mean of objective analyses, (b) observed SSH from the ESA SLCCI product, (c, e, g) mass SSH from GSFC RL05, JPL RL05 and JPL RL06 GRACE mascon products (which use Geruo A, Geruo A and ICE-6G GIA corrections respectively), (d, f, h) sum of steric and mass SSH from GSFC RL05, JPL RL05 and JPL RL06 mascon products respectively. Data are smoothed with a 500 km Gaussian filter for visualisation.

the updated pole tide correction and improved (RL06) AOD1B atmosphere-ocean dealiasing model.

The mass sea-level trend signal has more power at longer wavelengths than the observed SSHA trend signal due to the native resolution of the different observation systems (Figure 3). GRACE has a native resolution of 300 km (Vishwakarma et al., 2018) that is subsequently processed and filtered resulting in a longer wavelength effective resolution, whereas satellite altimetry has a minimum native resolution of 7 km along-track, which once filtered and processed to the multi-mission product has an effective resolution of between 100 and 800 km (latitude dependant; Ballarotta et al. (2019)). We might expect that the steric sea-level trend signal will capture the shorter wavelengths in the observed SSHA trend data, but that is not the case for the ensemble mean steric sea-level trend data set (Figure 3a). As a consequence the observed SSHA trend signal shows coherency with the discrepancy at wavelengths less than 1,000 km (Figure 3c). This means that the satellite altimetry product contains information not observed by the steric and mass products. At a global scale, there is coherency between the discrepancy in the SLB and both the altimetry and mass sea-level trends, indicating that systematic errors in orbit determination, geocenter motion (degree-1 spherical harmonics) and other low degree harmonics are also contributing to the difference. Therefore, it appears that the sampling bias of the steric observations and our smoothing by taking an ensemble mean of the optimal-interpolation products, combined with the native resolution of the GRACE observations, means the observations of steric and mass sea-level trend cannot provide any further information at this time towards the spatial SLB.

Given the spatial variability of the discrepancy, we aggregate onto basin-scale means to compare basin-scale SLBs. It is often stated that a significant contribution to the SLB

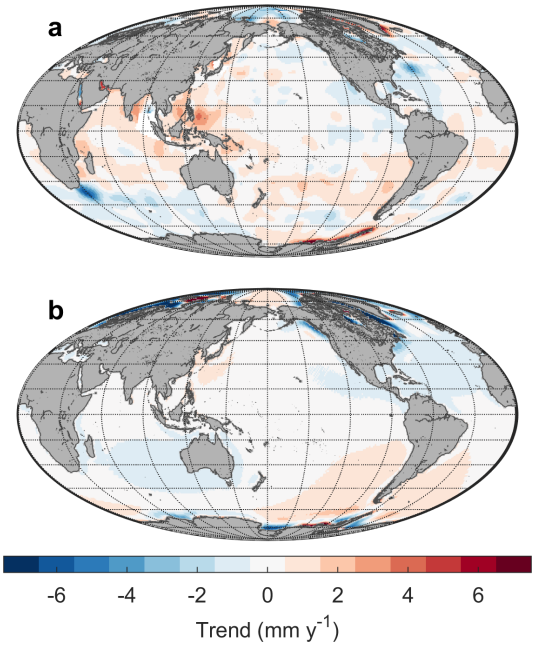

Figure 2. The mass SSH trend (mm y^{-1}) from (a) discrepancy between observed SSH trend from satellite altimetry (ESA SLCCI product) and the sum of steric (ensemble mean) and mass SSH trends (JPL RL06 with ICE-6G GIA), and (b) the difference between the Geruo A and ICE-6G GIA forward-model corrections for GRACE, as a trend in the equivalent water height.

discrepancy is due to the different sampling characteristics of steric and altimetry sea-level variations in eddy rich areas, where the reference track of the satellite altimeter may overpass more cold than warm eddies (or vice versa) and/or the ARGO float may become trapped in an eddy for sufficient time to bias observations low (or high) (von Schuckmann et al., 2014). This is expected to be a particular issue when using a linear trend to characterise the SLB, since the step in sea level between cold and warm eddy centers causes a spurious trend (see Hughes & Williams (2010) for a discussion of the high kurtosis in SSHA time series in eddy rich regions). To test the influence of these eddy rich areas on the basin-mean SLB, we have applied two different masks to the data sets: a 300 km buffer from land typically applied to GRACE data (Chambers (2006, 2009); WCRP (2018); Figure 4a) and a mask that removes data points that are poorly sampled by ARGO or by satellite altimetry or exhibit high variance typical of eddy rich regions (Figure 4b). It is noted that the buffer approach also removes shallow sea areas where steric changes are poorly sampled and observed SSHA from altimetry can contain larger errors. The latter masking approach is defined by data points where the standard deviation of the satellite altimetry SSHA or steric SLA monthly time series is greater than 150 mm or where the steric gridded time-series have less than 50% of time with a temperature and salinity profile located within 3 degrees longitude or latitude.

The basin-scale SLB closes in several basins when taking a time series mean (Figure 4), but fails to close within the uncertainty estimates for the Indian-South Pacific Ocean region. We find that masking those eddy rich or poorly sampled regions does not improve the SLB for this region (Figure 4d) but does marginally improve the SLB for the Sub-Polar and Sub-Tropical North Atlantic (Figure 4f,g) and North-West Pacific (Figure 4h). Our processing choices result in different global-mean sea-level trend values compared to previous studies (Table 3). We provide details of the basin-scale SLB with calculation method and product used in Supplementary Table S1.

Table 1. Basin-Mean and Global-Mean Sea-Level Trend by Calculation Method.

Product	Region						Global
	S Atl	Ind-S Pac	E Pac	SP N Atl	ST N Atl	NW Pac	
300 km buffer, time series mean							
EM steric[a]	1.2 ± 0.1	1.9 ± 0.1	2.0 ± 0.7	-0.5 ± 0.2	3.3 ± 0.5	-2.2 ± 0.4	1.1 ± 0.1
JPL RL06 ICE6G	1.8 ± 0.2	1.1 ± 0.2	2.3 ± 0.2	1.1 ± 0.2	2.5 ± 0.2	2.2 ± 0.2	1.8 ± 0.1
EM steric + JPL RL06 ICE6G	2.9 ± 0.3	3.0 ± 0.2	4.3 ± 0.7	0.7 ± 0.3	5.8 ± 0.5	0.0 ± 0.5	2.8 ± 0.1
ESA SLCCI	3.0 ± 0.2	4.6 ± 0.1	5.0 ± 0.8	0.5 ± 0.2	5.4 ± 0.5	0.6 ± 0.4	3.5 ± 0.1
High quality data only, time series mean							
EM steric[a]	1.0 ± 0.1	2.2 ± 0.1	1.9 ± 0.7	-0.5 ± 0.2	3.2 ± 0.4	-2.9 ± 0.5	1.0 ± 0.1
JPL RL06 ICE6G	1.7 ± 0.2	1.1 ± 0.1	2.4 ± 0.2	1.1 ± 0.2	2.2 ± 0.2	2.2 ± 0.2	1.7 ± 0.1
EM steric + JPL RL06 ICE6G	2.7 ± 0.3	3.3 ± 0.2	4.3 ± 0.8	0.6 ± 0.3	5.4 ± 0.5	-0.7 ± 0.5	2.7 ± 0.1
ESA SLCCI	3.2 ± 0.2	5.0 ± 0.1	5.0 ± 0.9	0.4 ± 0.2	5.8 ± 0.4	-0.2 ± 0.4	3.7 ± 0.1
300 km buffer, spatial mean							
EM steric[a]	1.2 ± 0.7	1.9 ± 0.8	1.9 ± 1.1	-0.5 ± 0.6	3.3 ± 1.1	-2.3 ± 1.0	1.1 ± 0.8
JPL RL06 ICE6G	1.8 ± 0.4	1.1 ± 0.4	2.3 ± 0.3	1.1 ± 0.3	2.5 ± 0.3	2.2 ± 0.3	1.8 ± 0.4
EM steric + JPL RL06 ICE6G	3.0 ± 0.8	2.9 ± 0.9	4.3 ± 1.1	0.6 ± 0.7	5.8 ± 1.2	-0.1 ± 1.1	2.8 ± 0.8
ESA SLCCI	3.0 ± 1.4	4.6 ± 1.5	5.0 ± 1.4	0.5 ± 1.0	5.4 ± 2.3	0.6 ± 1.7	3.5 ± 1.4

Note: Sea-level trend and 1 σ trend error estimate, Jan 2005--Dec 2015 (mm y^{-1})

[a]: Ensemble mean of 4 optimal-interpolation steric products

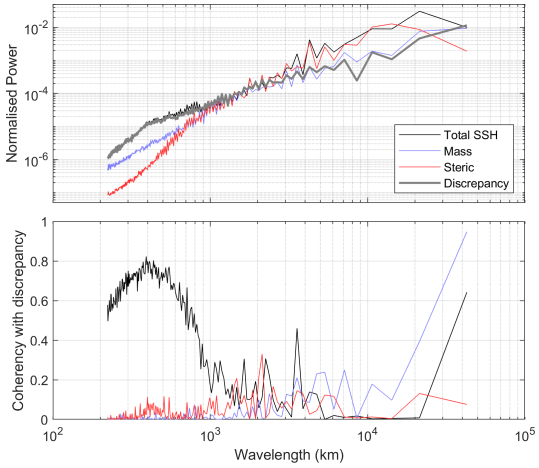

Figure 3. The wavelength spectra of (a) observed SSH (black), steric (red) and mass (blue) trends, and the discrepancy between the observed and steric plus mass SSH trends (grey), and (b) the cross-coherency of the wavelength spectra of the total, steric and mass trends with the discrepancy.

Global scale studies compare time series and their trend, area-weighted and averaged over the global ocean. So the time series obtained for each observation depends on the scale of the observation method. When comparing local to regional scale observations (at each grid point) this is a different mathematical problem where we are comparing observations spatially. Comparing the spatial mean of sea-level trends at a grid point gives different values than the linear trend of a spatial-mean time series (Figure 4). This is because outlier time series are smoothed out by the averaging process differently by taking the area-weighted time series, which gives a more robust trend fit, than by taking the area-weighted mean of individual time series trends, which by definition are noisier. In taking the time series trend, the seasonality across latitudes is lost, the area-weighting means the larger area of the tropics outweighs mid-latitude contributions but larger anomalies can dominate smaller anomalies in the mean. Whereas by taking the spatial-mean of sea-level trends, trends from grid points in the tropics dominate because of the area-weighting. Generally, SSHA in the tropics (particularly in the Indian and Pacific Oceans) is dominated by climatic teleconnections such as the El Niño Southern Oscillation (ENSO; see for example Cheng et al. (2008); Zhang & Church (2012); Palanisamy et al. (2015); Frankcombe et al. (2015); Thompson et al. (2016b)). Neither approach truly represents local-scale sea-level variability at the coast, which is affected by coastal processes as well as basin-scale mass redistribution and steric processes. However, it should be noted that the magnitude of the discrepancy between the observed SSHA trend and the sum of the steric and mass sea-level trends is generally smaller when taking a spatial-mean of the trends; but the uncertainties in the spatial-mean are higher because the uncertainties in each grid-point trend is high due to the noisier time series.

It is apparent that the largest coherence between the discrepancy in the SLB is with the observed SSHA trend at wavelengths less than 1,000 km (Figure 3) and that time series mean trends at the basin-scale are closer to closing the regional SLB than spatial-mean trends (Figure 4). This implies that neither the steric nor the mass observation systems have sufficient effective spatial resolution to match that of the observed SSHA from a satellite altimetry multi-mission product, which has an effective spatial resolution between 100 and 800 km (Ballarotta et al., 2019). If the SSHA variability were spatially random, we might expect the errors on these small scales to cancel over the basin-mean, but this does not appear to be the case for the time period and basins chosen in

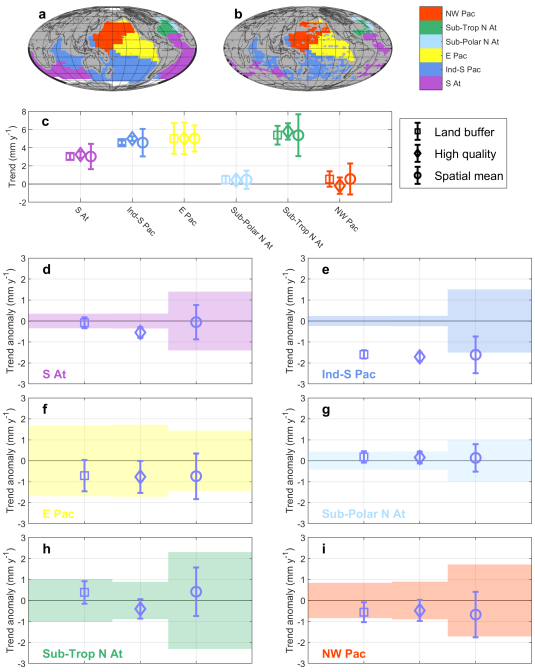

Figure 4. Sensitivity of SSH trend (mm y^{-1}) to spatial masking and method of trend calculation. (a) Ocean regions defined by Thompson & Merrifield (2014) with the 300 km land buffer masked in grey, (b) ocean regions with the 300 km buffer from land and poor data coverage or high variability masked in grey, (c) observed SSH trend from satellite altimetry (coloured by region) and (d-i) trend anomaly between the sum of ensemble mean steric and JPL RL06 mass SSH trend, and ESA SLCCI satellite altimetry SSH trend. Error bars in (c-i) and shaded regions in (d-i) represent 2σ formal trend error estimates for the satellite-altimetry and quadratic sum of mass and steric formal error estimates. The regional trends are ordered as (d) South Atlantic, (e) Indian-South Pacific, (f) East Pacific, (g) Subpolar North Atlantic, (h) Subtropical North Atlantic and (i) North-West Pacific.

this study. Similar results are found for simple Atlantic, Pacific and Indian Ocean basins (as defined by Chambers & Willis (2009)) and hence we conclude our results are robust to the basins chosen (see Supplementary Information). It appears that both the steric and mass derived sea-level provide good estimates of the SSHA trend processes, and the discrepancy in the SLB spatially appears to be due to (1) the effective spatial resolution of the steric and mass observations being too large; and, (2) differences between the mass and altimetry products due to processing choices made that affect the hemispherical scale.

We note there are processes missing in this analysis. Deep steric contributions are estimated to be between 0 and 0.3 mm y^{-1} at the global scale (Llovel et al., 2013; Dieng et al., 2015; Legeais et al., 2016), but there is thought to be considerable regional variability (Storto et al., 2017), with the most prominent impact probably in the southern ocean (Legeais et al., 2016).

Several studies have shown estimating ocean mass from GRACE data to be problematic for some ocean basins. Marcos et al. (2011) found the correlation of steric-corrected SSHA and GRACE ocean mass deseasoned sea-level residual (2004-2009) was particularly poor for the Indian Ocean and equatorial oceans. von Schuckmann et al. (2014) found the signal-to-noise ratio of GRACE ocean mass to be low in the equatorial oceans. Purkey et al. (2014) compared GRACE ocean mass with steric-corrected SSH at hydrographic

sections and aggregated into basin means, and concluded that the GRACE ocean mass overestimates in the North Pacific and underestimates in the Indian and South Pacific Oceans, outwith the 90% confidence intervals. These studies all used earlier releases of the GRACE data. Here, we find that the RL06 JPL mascon product shows a significant improvement over the RL05 on the basin-scale (Figure 4) but there remains a discrepancy outside of the 95% confidence limits for the Indian-South Pacific Ocean. Masking (and hence omitting from analysis) the most poorly sampled and high variability regions, which includes large parts of the Southern Ocean, makes little difference (Figure 4). Therefore, the discrepancy is not simply due to random errors in the sampling between the different observation systems.

4 Conclusions

The failure of the SLB to close on the basin scale for all basins, implies that the closure of the global-mean SLB may represent a cancellation of errors. Therefore, the true uncertainty in the measurements and/or the processes included in the SLB equation need careful consideration and further study.

In particular, the SLB does not close in the Indian-South Pacific region for any combination of data processing, masking and trend calculation method investigated in this study. For basin-mean trends calculated from the spatial-mean of trends, there is more uncertainty because the trend estimates are obtained from noisier time series data and therefore the formal trend error is larger, which puts further doubt on the SLB closure.

Whilst the SLB closes on the global scale, it is entirely plausible that taking the spatial mean time series averages out basin-scale systematic errors. Spatially, uncertainties in the altimetry and mass observation systems at the hemispheric scale and a lack of effective spatial resolution at scales less than 1,000 km in the steric and mass observation systems appear to dominate the discrepancy in the SLB. Therefore, a combination of sampling bias between the observation systems and systematic errors persist. At the length scales for which the observation systems were designed, the sum of steric and mass sea-level trend matches that measured by altimetry well for all ocean basins except the Indian-South Pacific region. The design of the observational systems therefore limits how informative the SLB can be at spatial scales less than 1,000 km but also raises the question of systematic errors of the order of 1 mm y^{-1} remaining at basin-scales in one or more of the observation systems, even with recent improvements to the processing methods.

Acknowledgments

The authors were all supported by European Research Council (ERC) under the European Union's Horizon 2020 research and innovation programme under grant agreement No 694188, the GlobalMass project (`globalmass.eu`). JLB was additionally supported through a Leverhulme Trust Fellowship (RF-2016-718) and a Royal Society Wolfson Research Merit Award.

The authors are grateful for the open availability of observational data sets, as referenced in the text, and to the developers of Generic Mapping Tools `http://gmt.soest.hawaii.edu/projects/gmt`. We are particularly grateful to Phil Thompson and Mark Merrifield for supplying their coherent SSH region mask.

GRACE Mascon data are available at `http://grace.jpl.nasa.gov`, supported by the NASA MEaSUREs Program.

References

A, G., Wahr, J., & Zhong, S. (2013). Computations of the viscoelastic response of a 3-D compressible Earth to surface loading: an application to Glacial Isostatic Adjustment in Antarctica and Canada. *Geophysical Journal International*, *192*, 557-572. doi: 10.1093/gji/ggs030

Ablain, M., Cazenave, A., Larnicol, G., Balmaseda, M., Cipollini, P., Faugère, Y., ... Benveniste, J. (2015). Improved sea level record over the satellite altimetry era (1993-2010) from the climate change initiative project. *Ocean Science*, *11*(1), 67–82. Retrieved from `https://www.ocean-sci.net/11/67/2015/` doi: 10.5194/os-11-67-2015

Argus, D. F., Peltier, W. R., Drummond, R., & Moore, A. W. (2014). The antarctica component of postglacial rebound model ICE-6G_C (vm5a) based on GPS positioning, exposure age dating of ice thicknesses, and relative sea level histories. *Geophysical Journal International*, *198*(1), 537-563. Retrieved from `http://dx.doi.org/10.1093/gji/ggu140` doi: 10.1093/gji/ggu140

AVISO. (2018). *Ssalto DUACS global all-satellite mean sea level gridded product version sealevel_glo_sla_map_l4_rep_observations_008_027.* Retrieved 22 February 2018 from ftp via `www.aviso.altimetry.fr/en/data/products/sea-surface-height-products/global.html`.

Ballarotta, M., Ubelmann, C., Pujol, M.-I., Taburet, G., Fournier, F., Legeais, J.-F., ... Picot, N. (2019). On the resolutions of ocean altimetry maps. *Ocean Science Discussions*, *2019*, 1–27. Retrieved from `https://www.ocean-sci-discuss.net/os-2018-156/` doi: 10.5194/os-2018-156

Blazquez, A., Meyssignac, B., Lemoine, J., Berthier, E., Ribes, A., & Cazenave, A. (2018). Exploring the uncertainty in grace estimates of the mass redistributions at the earth surface: implications for the global water and sea level budgets. *Geophysical Journal International*, *215*(1), 415-430. Retrieved from `http://dx.doi.org/10.1093/gji/ggy293` doi: 10.1093/gji/ggy293

Bos, M. S., Williams, S. D. P., Araújo, I. B., & Bastos, L. (2014). The effect of temporal correlated noise on the sea level rate and acceleration uncertainty. *Geophysical Journal International*. Retrieved from `http://gji.oxfordjournals.org/content/early/2013/12/20/gji.ggt481.abstract` doi: 10.1093/gji/ggt481

Chambers, D. P. (2006). Observing seasonal steric sea level variations with GRACE and satellite altimetry. *Journal of Geophysical Research: Oceans*, *111*(C3). Retrieved from `https://agupubs.onlinelibrary.wiley.com/doi/abs/10.1029/2005JC002914` doi: 10.1029/2005JC002914

Chambers, D. P. (2009). Calculating trends from GRACE in the presence of large changes in continental ice storage and ocean mass. *Geophysical Journal International*, *176*(2), 415-419. Retrieved from `https://onlinelibrary.wiley.com/doi/abs/10.1111/j.1365-246X.2008.04012.x` doi: 10.1111/j.1365-246X.2008.04012.x

Chambers, D. P., & Willis, J. K. (2009). Low-frequency exchange of mass between ocean basins. *Journal of Geophysical Research: Oceans*, *114*(C11). Retrieved from `https://agupubs.onlinelibrary.wiley.com/doi/abs/10.1029/2009JC005518` doi: 10.1029/2009JC005518

Chambers, D. P., & Willis, J. K. (2010). A global evaluation of ocean bottom pressure from GRACE, OMCT, and steric-corrected altimetry. *Journal of Atmospheric and Oceanic Technology*, *27*(8), 1395-1402. Retrieved from `https://doi.org/10.1175/2010JTECHO738.1` doi: 10.1175/2010JTECHO738.1

Chen, J., Tapley, B., Save, H., Tamisiea, M. E., Bettadpur, S., & Ries, J. (2018). Quantification of ocean mass change using gravity recovery and climate experiment, satellite altimeter, and argo floats observations. *Journal of Geophysical Research: Solid Earth*, *123*(11), 10,212-10,225. Retrieved from `https://agupubs.onlinelibrary.wiley.com/doi/abs/10.1029/2018JB016095`

463 doi: 10.1029/2018JB016095
464 Cheng, X., Qi, Y., & Zhou, W. (2008). Trends of sea level variations in the IndoPa-
465 cific warm pool. *Glob. Planet. Change*, *63*, 57–66. doi: 10.1016/j.gloplacha.2008
466 .06.001
467 Church, J. A., Gregory, J. M., White, N. J., Platten, S. M., & Mitrovica, J. X.
468 (2011). Understanding and projecting sea level change. *Oceanography*, *24*. doi:
469 doi.org/10.5670/oceanog.2011.33
470 CSIRO. (2019). *Combined TOPEX Poseidon, Jason-1, Jason-2 OSTM, Jason-*
471 *3 near-global gridded monthly-average sea level product.* Retrieved 16 April 2019
472 from `http://www.cmar.csiro.au/sealevel/sl_data_cmar.html`.
473 Desai, S., Wahr, J., & Beckley, B. (2015, Dec 01). Revisiting the pole tide for and
474 from satellite altimetry. *Journal of Geodesy*, *89*(12), 1233–1243. Retrieved from
475 `https://doi.org/10.1007/s00190-015-0848-7` doi: 10.1007/s00190-015-0848
476 -7
477 Dieng, H. B., Cazenave, A., von Schuckmann, K., Ablain, M., & Meyssignac, B.
478 (2015). Sea level budget over 20052013: missing contributions and data errors.
479 *Ocean Science*, *11*(5), 789–802. Retrieved from `https://www.ocean-sci.net/11/`
480 `789/2015/` doi: 10.5194/os-11-789-2015
481 Farrell, W. E., & Clark, J. A. (1976). On postglacial sea level. *Geophysical Jour-*
482 *nal of the Royal Astronomical Society*, *46*(3), 647-667. Retrieved from `https://`
483 `onlinelibrary.wiley.com/doi/abs/10.1111/j.1365-246X.1976.tb01252.x`
484 doi: 10.1111/j.1365-246X.1976.tb01252.x
485 Frankcombe, L. M., McGregor, S., & England, M. H. (2015). Robustness of the
486 modes of Indo-Pacific sea level variability. *Climate Dynamics*, *45*(5), 1281–1298.
487 Retrieved from `http://dx.doi.org/10.1007/s00382-014-2377-0` doi: 10.1007/
488 s00382-014-2377-0
489 Frederikse, T., Riva, R., Kleinherenbrink, M., Wada, Y., van den Broeke, M.,
490 & Marzeion, B. (2016). Closing the sea level budget on a regional scale:
491 Trends and variability on the northwestern european continental shelf. *Geo-*
492 *physical Research Letters*, *43*(20), 10,864-10,872. Retrieved from `https://`
493 `agupubs.onlinelibrary.wiley.com/doi/abs/10.1002/2016GL070750` doi:
494 10.1002/2016GL070750
495 Frederikse, T., Riva, R. E. M., & King, M. A. (2017). Ocean bottom deformation
496 due to present-day mass redistribution and its impact on sea level observations.
497 *Geophysical Research Letters*, *44*(24), 12,306-12,314. doi: 10.1002/2017GL075419
498 Gaillard, F., Reynaud, T., Thierry, V., Kolodziejczyk, N., & von Schuckmann, K.
499 (2016). In situbased reanalysis of the global ocean temperature and salinity with
500 isas: Variability of the heat content and steric height. *Journal of Climate*, *29*(4),
501 1305-1323. Retrieved from `https://doi.org/10.1175/JCLI-D-15-0028.1` doi:
502 10.1175/JCLI-D-15-0028.1
503 Goddard Space Flight Center. (2017). *Grace rl05 solution version v02.4.* Retrieved
504 15 November 2017 from `grace.jpl.nasa.gov/data/get-data/`.
505 Good, S. A., Martin, M. J., & Rayner, N. A. (2013). En4: Quality controlled ocean
506 temperature and salinity profiles and monthly objective analyses with uncertainty
507 estimates. *Journal of Geophysical Research: Oceans*, *118*(12), 6704-6716. Re-
508 trieved from `https://agupubs.onlinelibrary.wiley.com/doi/abs/10.1002/`
509 `2013JC009067` doi: 10.1002/2013JC009067
510 Gouretski, V., & Reseghetti, F. (2010, June). On depth and temperature biases in
511 bathythermograph data: Development of a new correction scheme based on analy-
512 sis of a global ocean database. *Deep Sea Research Part I: Oceanographic Research*,
513 *57*, 812-833. doi: 10.1016/j.dsr.2010.03.011
514 Hosoda, S., Ohira, T., & Nakamura, T. (2008). *A monthly mean dataset of global*
515 *oceanic temperature and salinity derived from Argo float observations* (Tech. Rep.
516 No. 8). JAMSTEC: JAMSTEC Rep. Res. Dev.

Hughes, C. W., & Williams, S. D. P. (2010). The color of sea level: Importance of spatial variations in spectral shape for assessing the significance of trends. *Journal of Geophysical Research: Oceans*, *115*(C10), n/a–n/a. Retrieved from http://dx.doi.org/10.1029/2010JC006102 (C10048) doi: 10.1029/2010JC006102

Jeon, T., Seo, K.-W., Youm, K., Chen, J., & Wilson, C. R. (2018). Global sea level change signatures observed by GRACE satellite gravimetry. *Scientific Reports*, *8*. doi: 10.1038/s41598-018-31972-8

JPL. (2018). *Grace rl05 solutions.* Retrieved 3 December 2018 from grace.jpl.nasa.gov/data/get-data/.

Kleinherenbrink, M., Riva, R., Frederikse, T., Merrifield, M., & Wada, Y. (2017). Trends and interannual variability of mass and steric sea level in the Tropical Asian Seas. *Journal of Geophysical Research: Oceans*, *122*(8), 6254-6276. Retrieved from https://agupubs.onlinelibrary.wiley.com/doi/abs/10.1002/2017JC012792 doi: 10.1002/2017JC012792

Kleinherenbrink, M., Riva, R., & Sun, Y. (2016). Sub-basin-scale sea level budgets from satellite altimetry, Argo floats and satellite gravimetry: a case study in the North Atlantic Ocean. *Ocean Science*, *12*(6), 1179–1203. Retrieved from https://www.ocean-sci.net/12/1179/2016/ doi: 10.5194/os-12-1179-2016

Legeais, J.-F., Ablain, M., Zawadzki, L., Zuo, H., Johannessen, J. A., Scharffenberg, M. G., ... Benveniste, J. (2018). An improved and homogeneous altimeter sea level record from the esa climate change initiative. *Earth System Science Data*, *10*(1), 281–301. Retrieved from https://www.earth-syst-sci-data.net/10/281/2018/ doi: 10.5194/essd-10-281-2018

Legeais, J.-F., Prandi, P., & Guinehut, S. (2016). Analyses of altimetry errors using argo and grace data. *Ocean Science*, *12*(3), 647–662. Retrieved from http://www.ocean-sci.net/12/647/2016/ doi: 10.5194/os-12-647-2016

Leuliette, E. W., & Willis, J. K. (2011). Balancing the sea level budget. *Oceanography*, *24*, 122-129. doi: 10.5670/oceanog.2011.32

Llovel, W., Fukumori, I., & B.Meyssignac. (2013). Depth-dependent temperature change contributions to global mean thermosteric sea level rise from 1960 to 2010. *Global and Planetary Change*, *101*, 113 - 118. doi: https://doi.org/10.1016/j.gloplacha.2012.12.011

Llovel, W., Guinehut, S., & Cazenave, A. (2010). Regional and interannual variability in sea level over 2002–2009 based on satellite altimetry, Argo float data and GRACE ocean mass. *Ocean Dynamics*, *60*(5), 1193–1204. Retrieved from https://doi.org/10.1007/s10236-010-0324-0 doi: 10.1007/s10236-010-0324-0

Llovel, W., Meyssignac, B., & Cazenave, A. (2011). Steric sea level variations over 20042010 as a function of region and depth: Inference on the mass component variability in the North Atlantic Ocean. *Geophysical Research Letters*, *38*(15), n/a – n/a. Retrieved from https://agupubs.onlinelibrary.wiley.com/doi/abs/10.1029/2011GL047411 doi: 10.1029/2011GL047411

Luthke, S. B., Sabaka, T. J., Loomis, B. D., Arendt, A. A., McCarthy, J. J., & Camp, J. (2013). Antarctica, Greenland and Gulf of Alaska land ice evolution from an iterated GRACE global mascon solution. *Journal of Glaciology*, *59*(216), 613–631. doi: 10.3189/2013JoG12J147

Marcos, M., Calafat, F. M., Llovel, W., Gomis, D., & Meyssignac, B. (2011). Regional distribution of steric and mass contributions to sea level changes. *Global and Planetary Change*, *76*(3), 206 – 218. Retrieved from http://www.sciencedirect.com/science/article/pii/S0921818111000166 doi: https://doi.org/10.1016/j.gloplacha.2011.01.007

Millero, F. J., Feistel, R., Wright, D. G., & McDougall, T. J. (2008). The composition of standard seawater and the definition of the reference-composition salinity scale. *Deep Sea Research Part I: Oceanographic Research Papers*, *55*(1), 50 -

72. Retrieved from http://www.sciencedirect.com/science/article/pii/S0967063707002282 doi: https://doi.org/10.1016/j.dsr.2007.10.001

Palanisamy, H., Cazenave, A., Delcroix, T., & Meyssignac, B. (2015). Spatial trend patterns in the pacific ocean sea level during the altimetry era: the contribution of thermocline depth change and internal climate variability. *Ocean Dynamics*, *65*(3), 341–356. Retrieved from http://dx.doi.org/10.1007/s10236-014-0805-7 doi: 10.1007/s10236-014-0805-7

Peltier, W. R. (2018). *Stokes coefficients for the ICE-6G_C/D VM5a GIA forward model.* Retrieved 23 July 2018 from www.atmosp.physics.utoronto.ca/~peltier/data.php.

Peltier, W. R., Argus, D. F., & Drummond, R. (2015). Space geodesy constrains ice age terminal deglaciation: The global ice-6g_c (vm5a) model. *Journal of Geophysical Research: Solid Earth*, *120*(1), 450-487. Retrieved from https://agupubs.onlinelibrary.wiley.com/doi/abs/10.1002/2014JB011176 doi: 10.1002/2014JB011176

Purkey, S. G., Johnson, G. C., & Chambers, D. P. (2014). Relative contributions of ocean mass and deep steric changes to sea level rise between 1993 and 2013. *Journal of Geophysical Research: Oceans*, *119*(11), 7509-7522. Retrieved from https://agupubs.onlinelibrary.wiley.com/doi/abs/10.1002/2014JC010180 doi: 10.1002/2014JC010180

Roemmich, D., & Gilson, J. (2009, August). The 2004-2008 mean and annual cycle of temperature, salinity, and steric height in the global ocean from the Argo Program. *Progress in Oceanography*, *82*, 81-100. doi: 10.1016/j.pocean.2009.03.004

Roemmich, D., Gilson, J., Sutton, P., & Zilberman, N. (2016). Multidecadal change of the South Pacific gyre circulation. *Journal of Physical Oceanography*, *46*(6), 1871-1883. doi: 10.1175/JPO-D-15-0237.1

Royston, S., Watson, C. S., Legrsy, B., King, M. A., Church, J. A., & Bos, M. S. (2018). Sea-level trend uncertainty with Pacific climatic variability and temporally-correlated noise. *Journal of Geophysical Research: Oceans*, *123*(3), 1978-1993. Retrieved from https://agupubs.onlinelibrary.wiley.com/doi/abs/10.1002/2017JC013655 doi: 10.1002/2017JC013655

Storto, A., Masina, S., Balmaseda, M., Guinehut, S., Xue, Y., Szekely, T., ... Wang, X. (2017, Aug 01). Steric sea level variability (1993–2010) in an ensemble of ocean reanalyses and objective analyses. *Climate Dynamics*, *49*(3), 709–729. doi: 10.1007/s00382-015-2554-9

Tamisiea, M. E. (2011). Ongoing glacial isostatic contributions to observations of sea level change. *Geophysical Journal International*, *186*(3), 1036-1044. Retrieved from https://onlinelibrary.wiley.com/doi/abs/10.1111/j.1365-246X.2011.05116.x doi: 10.1111/j.1365-246X.2011.05116.x

Tapley, B., Bettadpur, S., Ries, J., Thompson, P., & Watkins, M. (2004). GRACE measurements of mass variability in the Earth system. *Science*, *305*, 503–505. doi: 10.1126/science.1099192

TEOS-10. (2008). *Release on the IAPWS Formulation 2008 for the Thermodynamic Properties of Seawater* (Tech. Rep.). IAPWS. Retrieved from www.teos-10.org

Thompson, P. R., & Merrifield, M. A. (2014). A unique asymmetry in the pattern of recent sea level change. *Geophysical Research Letters*, *41*(21), 7675-7683. Retrieved from https://agupubs.onlinelibrary.wiley.com/doi/abs/10.1002/2014GL061263 doi: 10.1002/2014GL061263

Thompson, P. R., Piecuch, C. G., Merrifield, M. A., McCreary, J. P., & Firing, E. (2016a). Forcing of recent decadal variability in the Equatorial and North Indian Ocean. *Journal of Geophysical Research: Oceans*, *121*(9), 6762-6778. Retrieved from https://agupubs.onlinelibrary.wiley.com/doi/abs/10.1002/2016JC012132 doi: 10.1002/2016JC012132

Thompson, P. R., Piecuch, C. G., Merrifield, M. A., McCreary, J. P., & Firing, E.

(2016b). Forcing of recent decadal variability in the Equatorial and North Indian Ocean. *Journal of Geophysical Research: Oceans*, n/a–n/a. Retrieved from http://dx.doi.org/10.1002/2016JC012132 doi: 10.1002/2016JC012132

Uebbing, B., Kusche, J., Rietbroek, R., & Landerer, F. W. (2019). Processing choices affect ocean mass estimates from GRACE. *Journal of Geophysical Research: Oceans*, *124*(2), 1029-1044. Retrieved from https://agupubs.onlinelibrary.wiley.com/doi/abs/10.1029/2018JC014341 doi: 10.1029/2018JC014341

Vishwakarma, B. D., Devaraju, B., & Sneeuw, N. (2018). What is the spatial resolution of GRACE satellite products for hydrology? *Remote Sensing*, *10*(852). doi: 10.3390/rs10060852

von Schuckmann, K., Sallée, J.-B., Chambers, D., Le Traon, P.-Y., Cabanes, C., Gaillard, F., ... Hamon, M. (2014). Consistency of the current global ocean observing systems from an Argo perspective. *Ocean Science*, *10*(3), 547–557. Retrieved from https://www.ocean-sci.net/10/547/2014/ doi: 10.5194/os-10-547-2014

Wahr, J., Nerem, R. S., & Bettadpur, S. V. (2015). The pole tide and its effect on grace time-variable gravity measurements: Implications for estimates of surface mass variations. *Journal of Geophysical Research: Solid Earth*, *120*(6), 4597-4615. Retrieved from https://agupubs.onlinelibrary.wiley.com/doi/abs/10.1002/2015JB011986 doi: 10.1002/2015JB011986

Watkins, M. M., Wiese, D. N., Yuan, D.-N., Boening, C., & Landerer, F. W. (2015). Improved methods for observing Earth's time variable mass distribution with GRACE using spherical cap mascons. *Journal of Geophysical Research: Solid Earth*, *120*(4), 2648–2671. doi: 10.1002/2014JB011547

WCRP, G. (2018). Global sea-level budget 1993–present. *Earth System Science Data*, *10*(3), 1551–1590. Retrieved from https://www.earth-syst-sci-data.net/10/1551/2018/ doi: 10.5194/essd-10-1551-2018

Weise, D. N., Landerer, F. W., & Watkins, M. M. (2016). Quantifying and reducing leakage errors in the jpl rl05m grace mascon solution. *Water Resources Research*, *52*, 7490–7502. doi: 10.1002/2016WR019344

Wessel, P., Smith, W. H. F., Scharroo, R., Luis, J. F., & Wobbe, F. (2013). Generic mapping tools: Improved version released. *EOS Trans. AGU*, *94*, 409–410.

Wiese, D. N., Yuan, D.-N., Boening, C., Landerer, F. W., & Watkins, M. M. (2018). *Jpl grace mascon ocean, ice, and hydrology equivalent water height release 06 coastal resolution improvement (cri) filtered version 1.0.* Retrieved 3 December 2018 from grace.jpl.nasa.gov/data/get-data/. doi: 10.5067/TEMSC-3MJC6

Wöppelmann, G., & Marcos, M. (2016). Vertical land motion as a key to understanding sea level change and variability. *Reviews of Geophysics*, *54*(1), 64–92. Retrieved from http://dx.doi.org/10.1002/2015RG000502 (2015RG000502) doi: 10.1002/2015RG000502

Zhang, X., & Church, J. A. (2012). Sea level trends, interannual and decadal variability in the Pacific Ocean. *Geophysical Research Letters*, *39*(21), n/a–n/a. Retrieved from http://dx.doi.org/10.1029/2012GL053240 (L21701) doi: 10.1029/2012GL053240

Zlotnicki, V., Qu, Z., & Willis, J. (2019). *MEaSUREs gridded sea surface height anomalies version 1812.* Retrieved 16 April 2019 from podaac.jpl.nasa.gov. doi: 10.5067/SLREF-CDRV2